# RETROFIT OPTIMIZATION OF BATTERY AIR COOLING BY CFD AND MACHINE LEARNING

Eero Immonen*, Janne Sovela and Samuli Ranta
Engineering and Business, Technology Industry
Turku University of Applied Sciences
Joukahaisenkatu 3, 20520 Turku, C-siipi, Finland
Email: *Eero.Immonen@turkuamk.fi

Kirill Murashko and Paula Immonen
Laboratory of Electrical Engineering
LUT University
Yliopistonkatu 34, 53850 Lappeenranta, Finland

**KEYWORDS**

Battery; Air cooling; Design optimization; Retrofit; Computational fluid dynamics; Random forest; Feature importance

**ABSTRACT**

We investigate a simulation methodology for systematically optimizing air cooling in an *existing* battery system by placement of passive components. The goal in such *retrofit* optimization is to achive design improvement by making as few and cheap changes in the original system as possible. Our methodology utilizes CFD for fluid flow and heat transfer modeling and machine learning for cause-effect assessment across binary design variables, such as wall placement for passive flow control. As an application, we consider computational optimization of air cooling in a scaled-down electric bus charging station battery system.

## I INTRODUCTION

### *I-A Background*

Battery systems are seen today as a promising alternative for fossil fuels in mobile machinery, for reducing carbon dioxide emissions. Indeed, the electric vehicle technology in consumer use is already relatively mature, and progress has also been reported in electrification of public transport (Valenti et al., 2017), as well as heavy machinery (Moreda, Muñoz-García, & Barreiro, 2016; Valenzuela Cruzat & Anibal Valenzuela, 2018). It is important to note that batteries are used in their charging stations, too, for power peak control among others (Li, Huang, Zhang, & Bao, 2017).

An industrial-scale battery often requires a separate cooling system that aims to keep the temperature across the battery cells below a threshold level, typically $40°$C-$60°$C, specified by the cell manufacturer. Excess heat is known to deteriorate the cell and reduce its lifetime (K. Xu, Zhang, Jow, Xu, & Angell, 2002). Consequently, the cooling system should also ensure that the temperature *variation between* the cells is minimal, in order to ensure that the cells wear out evenly within a battery (Wang, Tseng, Zhao, & Wei, 2014).

The design of a battery cooling system is non-trivial, because the design objectives are complex and contradictory. On the one hand, the cells should be efficiently and uniformly cooled. On the other hand, the cooling system should be cheap and easy to install and maintain in practical use. In mobile applications, also a low weight for the cooling system is an obvious pre-requsite. Battery cooling systems are typically designed by using Computational Fluid Dynamics (CFD), whereby designers attempt to find an optimum cooling medium as well as a means to distribute it around the cells; see e.g. (An, Chen, Zhao, & Gao, 2019; Xun, Liu, & Jiao, 2013) and the references therein. For a survey of modern battery cooling methodologies, we refer the reader to (Peng, Garg, Zhang, & Shui, 2017).

Air cooling is often preferred in practice, because it yields a simple-to-build system which is also lightweight and low-cost. Furthermore, the cooling medium (cold air) can, at least in principle, be distributed around the cells without additional ductwork. However, the heat capacity rates in air cooling are also typically quite low. This implies that flow control, i.e. guiding the cooling air efficiently, plays a pivotal role in battery air cooling system design. The fact that the heat transfer coefficient for *forced* convection is up to an order of magnitude larger than that for *natural* convection further necessitates air *motion* around the cells in an air-cooled battery.

### *I-B Contribution of the article*

Several computational approaches for optimizing battery air cooling have been proposed in the academic literature, e.g. (Li, He, & Ma, 2013; Na, Kang, Wang, & Wang, 2018; Wang et al., 2014; X. Xu & He, 2013). However, to the authors' knowledge, little research has been reported on optimizing *existing* battery systems. In such "retrofit" optimization scenarios, one attempts to improve an existing design by making minimal modifications, as the equipment may be in daily use or difficult to access in practice.

The purpose of this article is to investigate the degree to which retrofit battery air cooling system optimization can be carried out by using passive components alone, and whether this optimization can be systematically carried out by utilizing CFD and machine learning. This optimization problem is not an easy one, because one should be able to draw conclusions robustly from a relatively small subset of the vast number of all conceivable design alternatives. In addition, as illustrated in Subsection I-C below, even simple geometry optimization tasks that involve fluid flow are often nonlinear mathematical problems. In this article, we present a generic methodology attempting to address these challenges and, as an application, we consider a down-scaled electric

Communications of the ECMS, Volume 34, Issue 1,
Proceedings, ©ECMS Mike Steglich, Christian Mueller,
Gaby Neumann, Mathias Walther (Editors)
ISBN: 978-3-937436-68-5/978-3-937436-69-2(CD) ISSN 2522-2414

bus charging station battery built at Turku University of Applied Sciences.

### I-C Motivating example

In a simple retrofit flow optimization case, an existing design layout is modified to locally enhance or balance air flow by *passive* equipment, such as plate blockages and guide vanes. However, even this simple scenario is a nonlinear mathematical problem, with complex cause-effect interactions. This is illustrated in Figure 1, which displays the velocity field in a turbulent air flow CFD simulation (see Subsection II-A for details) across an array of 4 square objects. In both cases, the flow is specified as 1 m/s from left to right, extending to a virtual wind tunnel geometry with only the zone around the squares shown. The only difference between the two geometries is the baffle blockage connecting the squares on the right. Yet this small difference affects the entire flow field: Notice that not only downstream, but also flow conditions *upstream* from the blockage are affected, and that effects are seen away from the baffle.

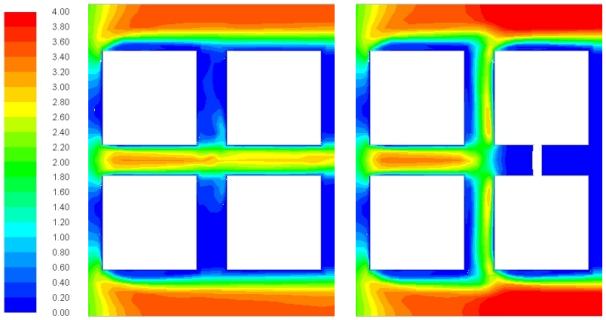


Fig. 1: Effect of Blockage on Flow Velocity Magnitude

## II METHODOLOGY

The retrofit design optimization methodology we consider in this article is based on fluid flow and heat transfer modeling by CFD and a systematic cause-effect assessment across binary design variables by machine learning. The details of this approach are given in this section, and the methodology is then applied for an existing battery system in the remainder of this article.

### II-A CFD modeling

#### 1) Fluid flow

We assume that air motion in the battery system is incompressible turbulent fluid flow, which is described by the Reynolds Averaged Navier-Stokes (RANS) equations in the steady state. In tensor notation, they read:

$$\frac{\partial \bar{u}_i}{\partial x_i} = 0 \tag{1}$$

$$\rho \frac{\partial (\bar{u}_i \bar{u}_j)}{\partial x_j} = -\frac{\partial p}{\partial x_i} + \frac{\partial}{\partial x_j}\left[2\mu \bar{S}_{ij} - \rho \overline{u_i' u_j'}\right] \tag{2}$$

with $\bar{S}_{ij} = \frac{1}{2}\left(\frac{\partial \bar{u}_i}{\partial x_j} + \frac{\partial \bar{u}_j}{\partial x_i}\right)$. Here $\mathbf{u} = (u_i, u_j, u_k)^T$ denotes the fluid velocity, $\rho$ denotes the (constant) fluid density, $p$ denotes pressure, and $\mu$ denotes dynamic viscosity. In addition, subscripts denote coordinates, and for any scalar quantity $a$, $\bar{a}$ denotes its time average and $a'$ denotes the fluctuating component in the Reynolds decomposition $a = \bar{a} + a'$.

The above equations require modification for any fan sections, as for design optimization it is not feasible to model fan blade motion directly. Instead, each fan zone constitutes a rotating reference frame, which yields a time-averaged (steady state) flow solution through the blades via the absolute velocity formulation.

To model turbulence, similar to the approach of (X. Xu & He, 2013), we assume that the Reynolds stresses $\rho \overline{u_i' u_j'}$ can be described via turbulence kinetic energy $k$ and its dissipation rate $\epsilon$, as in the $k-\epsilon$ turbulence model:

$$\rho \frac{\partial (k u_i)}{\partial x_i} = \frac{\partial}{\partial x_j}\left[\left(\mu + \frac{\mu_t}{\sigma_k}\right)\frac{\partial k}{\partial x_j}\right] + G - \rho\epsilon \tag{3}$$

$$\rho \frac{\partial (\epsilon u_i)}{\partial x_i} = \frac{\partial}{\partial x_j}\left[\left(\mu + \frac{\mu_t}{\sigma_\epsilon}\right)\frac{\partial \epsilon}{\partial x_j}\right] + C_{1\epsilon}\frac{\epsilon}{k}G - C_{2\epsilon}\rho\frac{\epsilon^2}{k} \tag{4}$$

where $G$ represents the effect of turbulence generation by velocity gradients, and $\mu_t = \rho C_\mu \frac{k^2}{\epsilon}$ represents eddy viscosity, which yields the Reynolds stresses via the Boussinesq hypothesis. We use the default constant values $C_{1\epsilon} = 1.44$, $C_{2\epsilon} = 1.92$, $C_\mu = 0.09$, $\sigma_k = 1.0$, and $\sigma_\epsilon = 1.3$ reported in the academic literature.

#### 2) Heat transfer

Heat transfer is described by the equation for conservation of energy $E$, for which each battery cell $c_k$ contributes as a local volumetric heat source $S_{c_k}$ (W/m$^3$):

$$\rho \nabla \cdot (\mathbf{u}E) = \nabla \cdot \left(\lambda \nabla T + \tau_{eff} \cdot \mathbf{u}\right) + \Sigma S_{c_k} \tag{5}$$

where $\lambda$ denotes thermal conductivity and $\tau_{eff} \cdot \mathbf{u}$ represents energy transfer by viscous dissipation.

### II-B Design optimization

The approach for CFD-based design optimization considered herein has two stages. In the first stage, a large batch of candidate designs, generated via statistical design of experiments, is simulated. In the second stage, the effect of each individual geometry modification on the design objective is estimated from this simulation data. The degree to which any given design variable improves or worsens the objective is estimated by employing the feature importance metric in the *random forest* machine learning scheme. Monte Carlo simulations help address the inherent stochasticity in the approach, as explained below.

#### 1) Design variables

We assume that there are $N$ locations in the air-cooled battery geometry model which can be blocked by introducing a *baffle plate*. As planar walls, they are easy to install, and their presence can be modeled as $N$ binary (on/off) design variables. In CFD simulations, such baffle plates can be modeled as infinitely thin walls. This facilitates using precisely the same computational mesh for simulating baffled design candidates as for simulating the present situation without baffles, i.e. the *baseline case*. It is well-known, see e.g. (Immonen, 2017), that this is important for drawing conclusions from the simulation

results: Even if the numerical values obtained from CFD calculations may have limited accuracy, one can more robustly infer which one of any two competing geometries performs better than the other.

*2) Fractional factorial designs*

For $N$ binary design variables, there are $2^N$ different combinations (the full factorial design), and evaluating them all becomes quickly impossible as $N$ increases. Fractional factorial designs (FFDs) are statistical design of experiments that are widely used for statistical cause-effect analyses (Pham, 2006). They are well known to efficiently exploit the fact that often many elements of the full factorial design are redundant (the sparsity-of-effects principle). Moreover, they facilitate controlling the degree of variable confounding, i.e. attributing an effect to some (combination of) design variables when in fact it is due to others. By definition, an FFD of resolution $R$ is one in which no $n$-factor interaction is confounded with any other effect containing less than $R–n$ factors.

*3) Feature importance by random forests*

Random forests are an ensemble-based machine learning method for classification and regression that operate by constructing a number of decision trees. Each tree attempts to model a subset of the full input-output relationship, and ensemble averaging aims to correct for decision trees' typical overfitting of the training set (Hastie, Tibshirani, & Friedman, 2009, pp. 587–588). For the retrofit battery air cooling system optimization problem, the inputs (or predictor variables) are the $N$ binary design variables, and the output (or response) is the global maximum cell temperature within the battery. Here, identification of a random forest model is carried out on the FFD batch data described in Subsection II-B2. For any given random forest, the predictor variable importances (i.e. their relative significance for the response) can be estimated by permuting out-of-bag observations among the trees (Loh, 2002).

*4) Monte Carlo simulation*

The outcome of a feature importance analysis for a given random forest, described in Subsection II-B3, not only depends on tree-forest structure (e.g. the number of trees, leaves etc.) but also on how the underlying input-output relation was partitioned across the trees in the random forest. Therefore, this outcome is stochastic. To address this, we consider a Monte Carlo simulation in which the feature importance analysis of Subsection II-B3 is carried out for several different random forest specifications. This yields a statistical description of the feature importances, and one can more robustly infer which (if any) of the design variables have the desired effect on the output.

## III APPLICATION: A DOWN-SCALED ELECTRIC BUS CHARGING STATION BATTERY SYSTEM

### *III-A The SeBNet battery system*

During the SeBNet project (*Smart Electric Bus Network Integration*, from 1.7.2017 to 31.12.2019), a student team at Turku University of Applied Sciences developed and built the initial down-scaled (1:10) version of an electric bus charging station battery system shown in Figure 2. It consists of a series connection of 16 LiFePO4 cells (GWL Power, 3.2 V, 20 Ah, 64 Wh, 0.65 kg), which must be kept below 45°C during charge and below 55°C during discharge, according to the manufacturer's specification. Further, the maximal continuous charge and discharge currents for the cells are 20A (1C) and 60A (3C), respectively. The cell's internal resistance is stated by the manufacturer to be less than 0.002 Ω. These yield an estimate of the maximum heat generation rate: $16 \times 7.2$ W = 115.2 W for the whole battery system. The two fans (Arctic F14PWM, each rated at 126 $m^3$/h) on the back panel, operated at the maximum rpm, attempt to remove this heat from the casing. In practical use, the air cooling system utilizes dry air at room temperature 20°C drawn through the front panel only; the top and bottom sections of the casing are sealed closed.

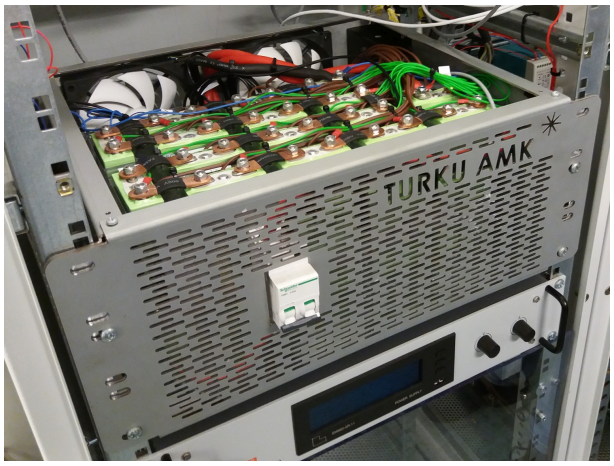


Fig. 2: The SeBNet Battery System

### *III-B Baseline CFD model development and simplifications*

*1) Geometry*

The CFD geometry model for the SeBNet battery system, adapted from the original SolidWorks design drawings, is displayed in Figure 3.

The 16 cells (shown in blue color in Figure 3) were modeled as 71 mm × 178 mm × 28 mm solid rectangular regions, as in the cell specification document. The cells are connected by rectangular solid busbars (shown in brown color in Figure 3). The CFD geometry model includes the battery management system, capacitors, relays and support structures as flow blocking objects. No wire connections were included in the CFD model because they only fill a relatively small part of the total battery volume and their exact locations is may change or even be unknown in practice.

*2) Mesh*

The computational mesh (i.e. spatial discretization) chosen for the model consists of approximately 601000 cells. A mesh sensitivity analysis was carried out, for meshes up to 5.2 million cells to ensure independence of the results on mesh resolution.

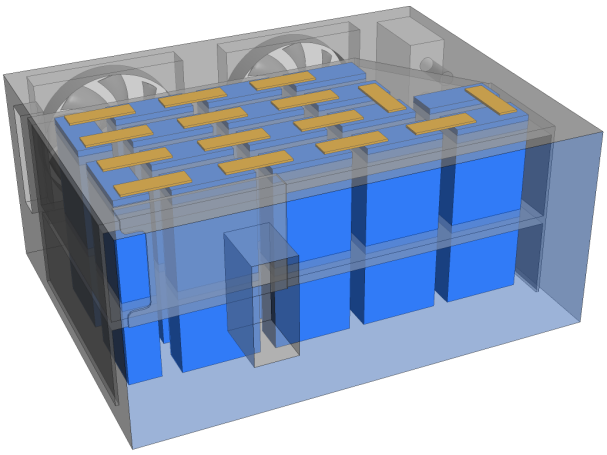

Fig. 3: The SeBNet Battery System CFD Geometry

*3) Casing*

The casing walls were assumed to be adiabatic.

*4) Fans*

The fan blades were modeled by hand as accurately as possible. To account for modeling errors, the fan speed in the simulations was calibrated to match the specified maximum volume flow rate of 126 $m^3$/h in virtual wind tunnel simulations (see Figure 4 for an example).

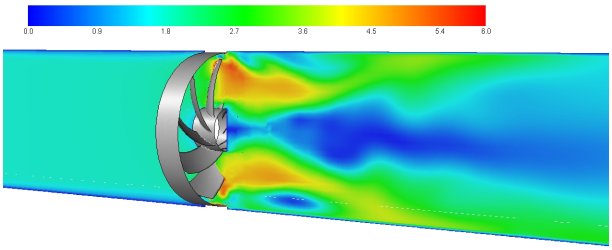


Fig. 4: Simulated Air Velocity in a Virtual Wind Tunnel (Fan Speed 1200 RPM)

*5) Front panel*

The front panel with TURKU AMK branding (cf. Figure 2) was modeled as a homogeneous inlet vent boundary yielding a pressure drop $\Delta p = k_L \frac{1}{2} \rho v^2$. The loss coefficient value $k_L = 21.5$ was obtained from virtual wind tunnel simulations, similar to the fans described in Subsection III-B4 above.

*6) Battery cells*

The internal structure and thermo-electric behavior of the cells was not modeled in detail. Instead, each battery is treated as a homogeneous volumetric heat source of 7.2 W. This corresponds to the maximum continuous discharge conditions with an infinite battery capacity, i.e. extremal use conditions from the practical point of view. The battery terminals were not included separately in the simulation model, as they are covered by the busbars.

*7) Materials*

The incoming air is treated as dry at 20°C, the busbars are made of copper and the LiFePO4 cells' thermal properties were obtained from the academic literature (Mathewson, 2014).

### *III-C Simulation environment and solver settings*

For CFD simulations, we utilized ANSYS Fluent 2019 R3 with the Coupled pressure-velocity scheme and second-order discretization everywhere except for turbulence, which was specified as the First Order Upwind scheme. All simulations were carried out on the "Puhti" supercomputer at CSC – IT Center for Science Ltd, Finland. Each case was simulated using 40 CPU cores and 10000 iterations. Such a high iteration count is necessary for reaching a steady state in the flow field, as especially convergence of the energy equation solution turned out to be slow. The simulation time for one case was approximately 50 minutes.

### *III-D Baseline model simulation results*

Figure 5 displays the simulated velocity magnitude profile within the battery system on two artificial perpendicular planes. Note that there is significant air flow through the opening *above* the cells, where there is little cell area exposed to cooling. Also note that there are higher and lower velocity regions between the cells, which causes some cells to be less effectively cooled than others.

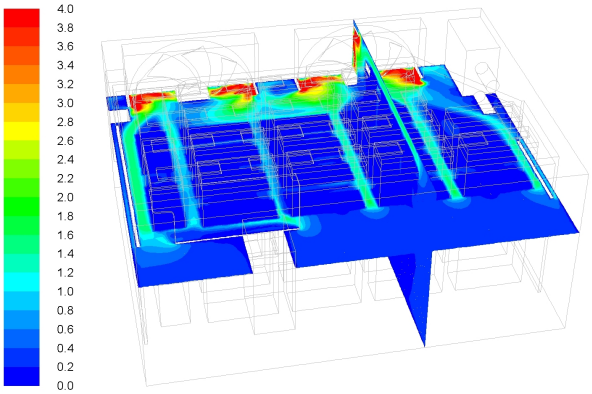


Fig. 5: Flow Velocity Magnitude (Baseline CFD)

Figure 6 displays the simulated temperature profile at an artificial midsection plane. Clearly there is significant variation between the cell temperatures. Moreover, the hottest cells are close to the low air velocity regions (cf. Figure 5).

### *III-E Model validation*

In order to validate the simulation model by measurements, the SeBNet battery system was first charged from 0% to 100% in 60 minutes at 1C (20A), then left to settle for 15 minutes, and finally discharged from 100% to 0% in 20 minutes at 3C (60A). Cell temperatures were continuously measured, with the temperature probes placed at the center of the large side on each cell.

Table I displays the simulated maximum cell temperatures (middle column) and the corresponding measured cell temperatures (right column). The average error

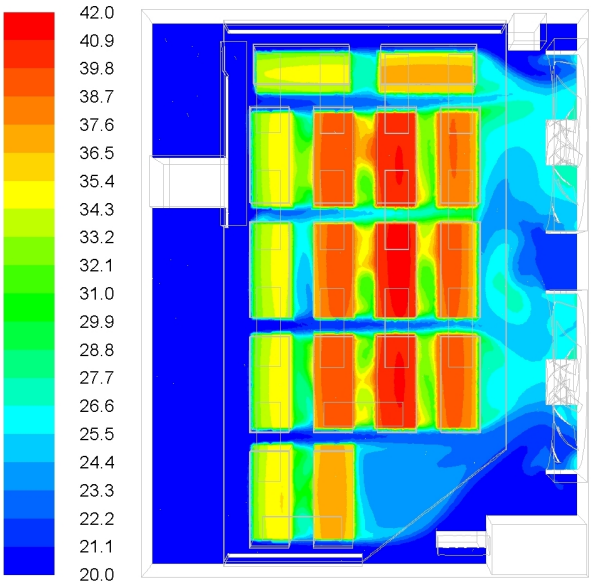


Fig. 6: Temperature (Baseline CFD)

between simulation results and measurements is $6\%$. We consider this accuracy reasonably good especially bearing in mind the differences between the simulation and measured cases: First of all, the measurements were not obtained from a steady state situation, but after a transient cycle. Second, the cells' internal resistances were measured, and they ranged from $1.81$ m$\Omega$ to $2.35$ m$\Omega$, which is grossly outside of the manufacturer's specification (below $2$ m$\Omega$). Finally, a comparison is made between the simulated *maximum* cell temperature and temperature measurement *at a specific location*.

## IV CFD OPTIMIZATION OF THE AIR COOLING SYSTEM

### *IV-A Retrofit design optimization*

#### *1) Baffle plate placement options*

In total $24$ possible baffle plate placement locations, shown in green color in Figure 7, were identified for the SeBNet model. This set of possible baffle locations is a compromise between computational simplicity and ability to guide the flow in complex patterns through the casing. In the optimum design, some of the $24$ zones are walls and the others are interior zones that are transparent to flow and heat transfer in CFD simulations.

#### *2) Design of experiments*

We used the Franklin-Bailey algorithm (Franklin & Bailey, 1977) implemented in MATLAB 2019b for constructing an FFD of resolution $4$. The resulting design-of-experiments was a binary $256 \times 24$ matrix, for which the elements of each row determined the subset of the $24$ baffles that was to be included as walls in the CFD simulation. This FFD is a compromise of simulation time and case comprehension: At resolution $4$, the design does not confound either main effects or two-way interactions but may confound two-way interactions (and beyond) with each other.

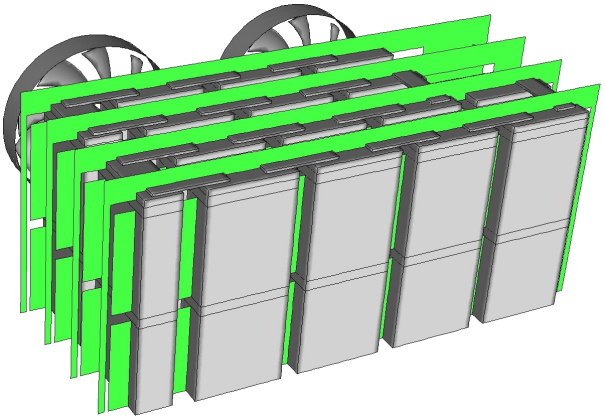

Fig. 7: Possible Baffle Plate Locations (Green).

#### *3) Effect of baffles 1-24 on cell temperatures*

Figure 8 shows the individual effects of the baffle plates $1-24$ on the global maximum cell temperature observed in the CFD simulations in the steady state. The underlying data is from the $256$ CFD simulation cases of the FFD. The boxplot shows the importance of the features across a Monte Carlo simulation of $2000$ iterations, with the random forest tree count ranging between $30-100$ (uniform distribution). Each random forest model was fitted using bootstrap aggregation in MATLAB 2019b (Breiman, 2001).

By Figure 8, only baffles $7$ and $8$ contribute to lowering the cell temperatures. These baffle plates are shown in Figure 9. For all other baffle plates, the boxplot maxima in Figure 8 extend above zero, indicating that they may not help reducing the maximum cell temperatures.

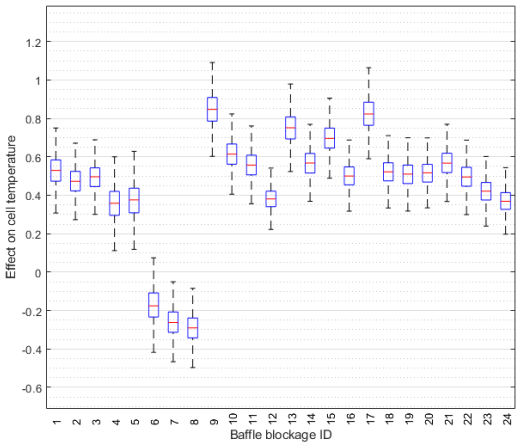


Fig. 8: Effect of Baffle Plates $1-24$ on Global Maximum Cell Temperature

### *IV-B Optimal design: Results and analysis*

#### *1) Optimal design*

In Subsection IV-A3, we concluded that only the baffles $7$ and $8$ could be expected to reduce the maximum cell temperature in the battery system. The *optimal design*

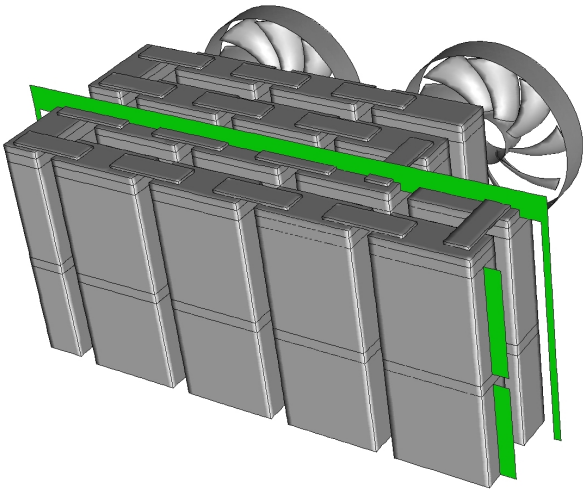

Fig. 9: Baffle Plate 7 (Two Vertical Sections on the First Row of Cells) and Baffle Plate 8 (Single Section Extending to the Top of the Second Row of Cells) Shown in Green

is thus that presented in Figure 9. In the remainder of this section, we show that it indeed displays a lower simulated global maximum temperature than in the baseline model. We also analytically study the fluid mechanics properties of the CFD simulation results for the optimal case.

*2) Optimal design simulation results*

Figure 10 displays the velocity magnitude profile within the battery system on the same two artificial perpendicular planes as in Figure 5, with baffles 7 and 8 now included as walls. In comparison to the baseline model (cf. Figure 5), there is no longer air flow through the compartment above the cells. The modifications yield higher flow speeds between the cells and potentially better cooling of the hottest cells of the baseline model.

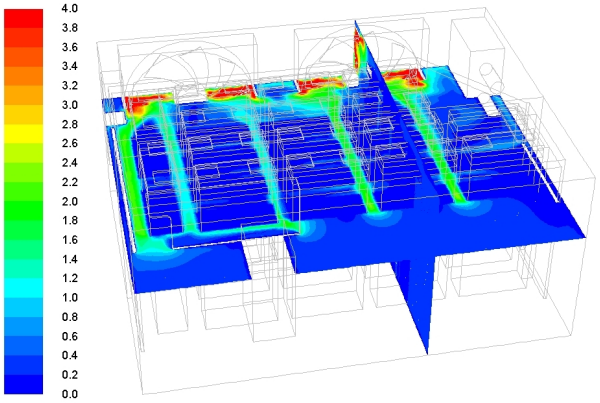


Fig. 10: Flow velocity magnitude (Optimal CFD)

The simulated maximum cell temperatures for the optimal design are shown in Table I (left column). In addition, Figure 11 displays the simulated temperature profile at the same artificial midsection plane as in Figure 6. In comparison to the baseline model (cf. Figure, 6), the highest simulated cell temperatures are indeed lower in the optimal design: The maximum cell temperature is reduced from $42.5°$C to $41.5°$C. The difference is clearly not a large one, and, moreover, some cells are hotter in the optimum design than in the baseline case. However, the design objective utilised in Subsection IV-A3 was specifically the reduction of the global maximum cell temperature, which was thus achieved.

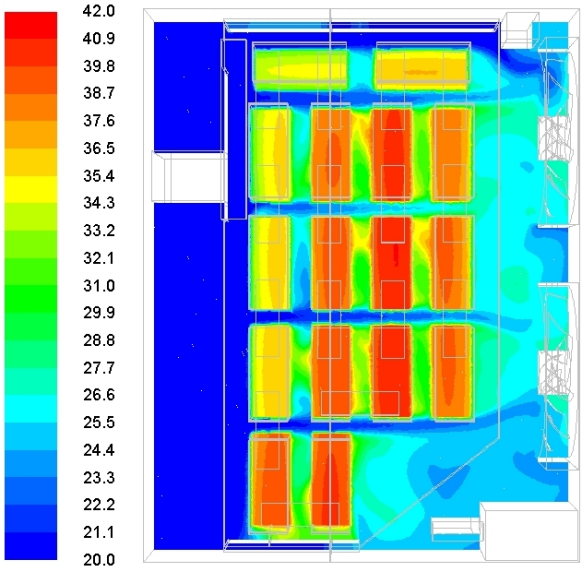


Fig. 11: Temperature (Optimal CFD)

TABLE I: Cell Temperatures in Simulations and Measurements

| Cell id | Optimal (CFD) | Baseline (CFD) | Baseline (measured) |
|---|---|---|---|
| **#1** | 39.3 | 39.6 | 41.8 |
| **#2** | 39.4 | 40.1 | 42.1 |
| **#3** | 38.9 | 39.5 | 42.4 |
| **#4** | 36.7 | 37.2 | 37.9 |
| **#5** | 40.9 | 42.2 | 43.5 |
| **#6** | 41.5 | 42.5 | 41.9 |
| **#7** | 41.2 | 41.8 | 40.8 |
| **#8** | 39.9 | 40.4 | 41.6 |
| **#9** | 39.6 | 40.2 | 37.8 |
| **#10** | 39.7 | 40.8 | 37.5 |
| **#11** | 35.3 | 35.0 | 37.7 |
| **#12** | 36.2 | 36.5 | 37.2 |
| **#13** | 36.2 | 35.8 | 37.6 |
| **#14** | 36.9 | 36.1 | 34.8 |
| **#15** | 39.9 | 36.2 | 40.3 |
| **#16** | 40.1 | 38.2 | 40.5 |

*3) Evaluation*

From fundamental thermodynamics, the heat transfer rate for an air-cooled battery system can be increased by increasing the rate of cooling air. However, introduction of baffles in the SeBNet battery system in fact *reduces* the total mass flow rate through the front panel, because they result in an additional pressure loss. This is seen in Figure 8: Most of the modifications yield an increase in the maximum cell temperature. Consequently, optimization of the SeBNet battery system by any baffle plate arrangement is challenging, which is reflected in the modest improvement achieved here relative to the baseline model.

## V CONCLUSIONS

In the present article, we have investigated a simulation-based methodology for optimizing air cooling in an *existing* battery system by passive components, such as baffle plates. We utilized CFD for fluid flow and heat transfer modeling and machine learning for cause-effect assessment across binary design variables. We demonstrated use of the methodology for a down-scaled electric bus charging station battery system. In this application, a simple combination of baffle plates resulting in a lower global maximum cell temperature was systematically extracted out of a vast set of $2^{24}$ design alternatives. Although the temperature reduction achieved was relatively small, the results indicate that the approach considered herein may be beneficial for retrofit design optimization. In future applications, one should not only consider introduction of blockages, but removing existing ones, for improved air circulation and better cooling efficiency. Moreover, future research on the methodology outlined in this article should focus on accounting for both the global maximum cell temperature and inter-cell temperature variation. The latter was not considered here.

## ACKNOWLEDGEMENTS

The authors gratefully acknowledge funding from Business Finland (e3Power project). The ability to use CSC's scientific computing facilities is also gratefully acknowledged.

## REFERENCES

An, Z., Chen, X., Zhao, L., & Gao, Z. (2019). Numerical investigation on integrated thermal management for a lithium-ion battery module with a composite phase change material and liquid cooling. *Applied Thermal Engineering*, *163*, 114345.

Breiman, L. (2001). Random forests. *Machine learning*, *45*(1), 5–32.

Franklin, M., & Bailey, R. (1977). Selection of defining contrasts and confounded effects in two-level experiments. *Journal of the Royal Statistical Society: Series C (Applied Statistics)*, *26*(3), 321–326.

Hastie, T., Tibshirani, R., & Friedman, J. (2009). *The elements of statistical learning: data mining, inference, and prediction*. Springer Science & Business Media.

Immonen, E. (2017). 2D shape optimization under proximity constraints by CFD and response surface methodology. *Applied Mathematical Modelling*, *41*, 508 - 529.

Li, Q., Huang, M., Zhang, W., & Bao, Y. (2017, Aug). Economic study on bus fast charging station with battery energy storage system. In *2017 IEEE ITEC Asia-Pacific Conference* (p. 1-6).

Li, X., He, F., & Ma, L. (2013). Thermal management of cylindrical batteries investigated using wind tunnel testing and computational fluid dynamics simulation. *Journal of Power Sources*, *238*, 395 - 402.

Loh, W.-Y. (2002). Regression tress with unbiased variable selection and interaction detection. *Statistica sinica*, 361–386.

Mathewson, S. (2014). *Experimental measurements of LiFePO4 battery thermal characteristics* (Unpublished master's thesis). University of Waterloo.

Moreda, G., Muñoz-García, M., & Barreiro, P. (2016). High voltage electrification of tractor and agricultural machinery–a review. *Energy Conversion and Management*, *115*, 117–131.

Na, X., Kang, H., Wang, T., & Wang, Y. (2018). Reverse layered air flow for li-ion battery thermal management. *Applied Thermal Engineering*, *143*, 257 - 262.

Peng, X., Garg, A., Zhang, J., & Shui, L. (2017, Oct). Thermal management system design for batteries packs of electric vehicles: A survey. In *2017 asian conference on energy, power and transportation electrification (ACEPT)* (p. 1-5).

Pham, H. (2006). *Springer handbook of engineering statistics*. Springer Science & Business Media.

Valenti, G., Liberto, C., Lelli, M., Ferrara, M., Nigro, M., & Villante, C. (2017, June). The impact of battery electric buses in public transport. In *2017 IEEE EEEIC / I CPS Europe conference* (p. 1-5).

Valenzuela Cruzat, J., & Anibal Valenzuela, M. (2018, Nov). Integrated modeling and evaluation of electric mining trucks during propel and retarding modes. *IEEE Transactions on Industry Applications*, *54*(6), 6586-6597.

Wang, T., Tseng, K., Zhao, J., & Wei, Z. (2014). Thermal investigation of lithium-ion battery module with different cell arrangement structures and forced air-cooling strategies. *Applied Energy*, *134*, 229 - 238.

Xu, K., Zhang, S., Jow, T. R., Xu, W., & Angell, C. A. (2002). Libob as salt for lithium-ion batteries: a possible solution for high temperature operation. *Electrochemical and Solid-State Letters*, *5*(1), A26–A29.

Xu, X., & He, R. (2013). Research on the heat dissipation performance of battery pack based on forced air cooling. *Journal of Power Sources*, *240*, 33 - 41.

Xun, J., Liu, R., & Jiao, K. (2013). Numerical and analytical modeling of lithium ion battery thermal behaviors with different cooling designs. *Journal of Power Sources*, *233*, 47 - 61.

## AUTHOR BIOGRAPHIES

**EERO IMMONEN** is an Adjunct Professor at Department of Mathematics at University of Turku, Finland, and works as Principal Lecturer at Turku University of Applied Sciences, Finland.

**JANNE SOVELA** works as Senior Advisor at New Energy Research Group at Turku University of Applied Sciences, Finland.

**SAMULI RANTA** works as Senior Lecturer and New Energy Research Group Leader at Turku University of Applied Sciences, Finland.

**KIRILL MURASHKO** works as Post-Doctoral Researcher at LUT University, Finland.

**PAULA IMMONEN** works as Post-Doctoral Researcher at LUT University, Finland.